Publ. Astron. Soc. Aust., 2000, 17, 234–240

Spectral Characteristics of the 2dFGRS–NVSS Galaxies

C. A. Jackson[1] and D. M. Londish[2]

[1]Research School of Astronomy & Astrophysics, Institute of Advanced Studies,
Australian National University, Canberra, ACT 0200, Australia
cjackson@mso.anu.edu.au
[2]School of Physics, University of Sydney, NSW 2006, Australia

Received 2000 April 6, accepted 2000 August 25

Abstract: We have analysed the 2dF spectra of a sample of galaxies common to the 2dF Galaxy Redshift Survey (2dFGRS, Colless 1999) and the NRAO VLA Sky Survey (NVSS, Condon et al. 1998). Our sample comprises 88 galaxies selected by Sadler et al. (1999) from 30 2dFGRS fields observed in 1998. In this paper we discuss how this and future, much larger, samples of 2dFGRS–NVSS galaxies can be interpreted via analysis of those galaxies with strong narrow emission lines. Using diagnostic line ratio measurements, we confirm the majority of the eyeball classifications of Sadler et al. (1999), although many galaxies show evidence of being 'composite' galaxies—mixtures of AGN plus starburst components.

Keywords: galaxies: evolution—galaxies: jets—quasars: general—radio continuum: galaxies

1 Introduction

Sources common to 2dFGRS and deep radio surveys (NVSS, FIRST, SUMSS)[1] comprise large samples of local, low-to-moderate power radio sources. The sheer number of objects (in the completed 2dFGRS, we expect ~4000 galaxies in common with NVSS) and the homogeneity of the spectra will allow us to make statistical studies of sub-populations among the radio sources, so revealing a much clearer picture of their properties (and perhaps identifying rare or new classes of objects). Most importantly, the overlap between 2dFGRS and NVSS provides a sample from which to derive the local radio luminosity function, as ~50% of these galaxies lie at $z <$ 0.1 (Sadler et al. 1999). A future paper will derive this local radio luminosity function and discuss the contributions of individual populations. This paper reports the results of an emission-line diagnostic analysis of the preliminary sample of 2dFGRS–NVSS galaxies, checking these against the intial 'eyeball' classifications of Sadler et al. (1999).

Throughout this paper values of $H_0 = 75$ km s^{-1} Mpc^{-1} and $\Omega = 1.0$ are used.

2 The Sample of 2dFGRS–NVSS Galaxies

The sample of 88 2dFGRS–NVSS galaxies has been extracted from the 2dFGRS and NVSS surveys, selecting sources whose radio–optical offset is less than 10 arcsec. Complete details of the selection criteria, cross-matching and classification procedures are described by Sadler et al. (1999). FITS files containing the reduced 2dF spectra for these galaxies were provided by the 2dFGRS project.

Each galaxy has an assigned spectral type of either 'S' = starburst or 'A' = AGN, defined as follows:

AGN have either a pure absorption-line spectrum, characteristic of an early-type galaxy, *or* an emission-line signature similar to those of optically-selected Seyferts, with dominant nebular emission lines (e.g. [OIII] and [OII]) relative to any Balmer-line emission. As Figure 1 shows, the majority of these objects have much lower radio powers than those usually associated with radio-loud AGN ($\log_{10}(P_{1.4\mathrm{GHz}}) \sim 10^{21} - 10^{24}$ W Hz^{-1} sr^{-1}).

We can describe these AGN in terms of two subclasses:

The absorption-line AGN have radio powers typical of FR I radio galaxies, and optical spectra typical of early-type host galaxies. These sources show none of the characteristic emission lines associated with star formation processes.

The emission-line AGN could be (i) 'radio-quiet' Seyfert 2s—late-type hosts with sub-pc-scale radio core-jet structures, (ii) emission-line FRI radio galaxies—rare but not unknown, or (iii) emission-line FR II radio galaxies, although this is unlikely as these are usually more powerful, $\log_{10}(P_{1.4\mathrm{GHz}}) \geq 10^{24}$ W Hz^{-1} sr^{-1}, and are rare at $z < 0.3$.

Starburst galaxies have emission-line signatures similar to those of optically-selected star-forming galaxies, with strong Balmer-line emission relative to any other emission features. Figure 2 shows that most of these objects are of low radio powers, $\log_{10}(P_{1.4\mathrm{GHz}}) \leq 10^{22}$ W Hz^{-1} sr^{-1}, typical of known starburst galaxies.

Our sample comprises 36 starburst galaxies and 52 AGN. At the time of this analysis, FITS data were unavailable for 3 of the 36 starburst galaxies. Of the remaining 33, 22 have both Hα and Hβ in emission within the 2dFGRS wavelength range (i.e. they lie at $z <$ 0.2). The 52 AGN can be subdivided into one broad-line Seyfert 1, 40 absorption-line (early-type) galaxies, one galaxy at $z > 0.2$, and 10 with both Hα and Hβ in emission (and $z < 0.2$). The 22 starburst galaxies and 10

[1] NVSS: the NRAO VLA Sky Survey at 1.4 GHz, Condon et al. (1998); FIRST: Faint Images of the Radio Sky at 20 cm, White et al. (1997); SUMSS: the Sydney University Molonglo Sky Survey at 843 MHz, Bock, Large & Sadler (1999).

 10.1071/AS00042 1323-3580/00/030234$05.00

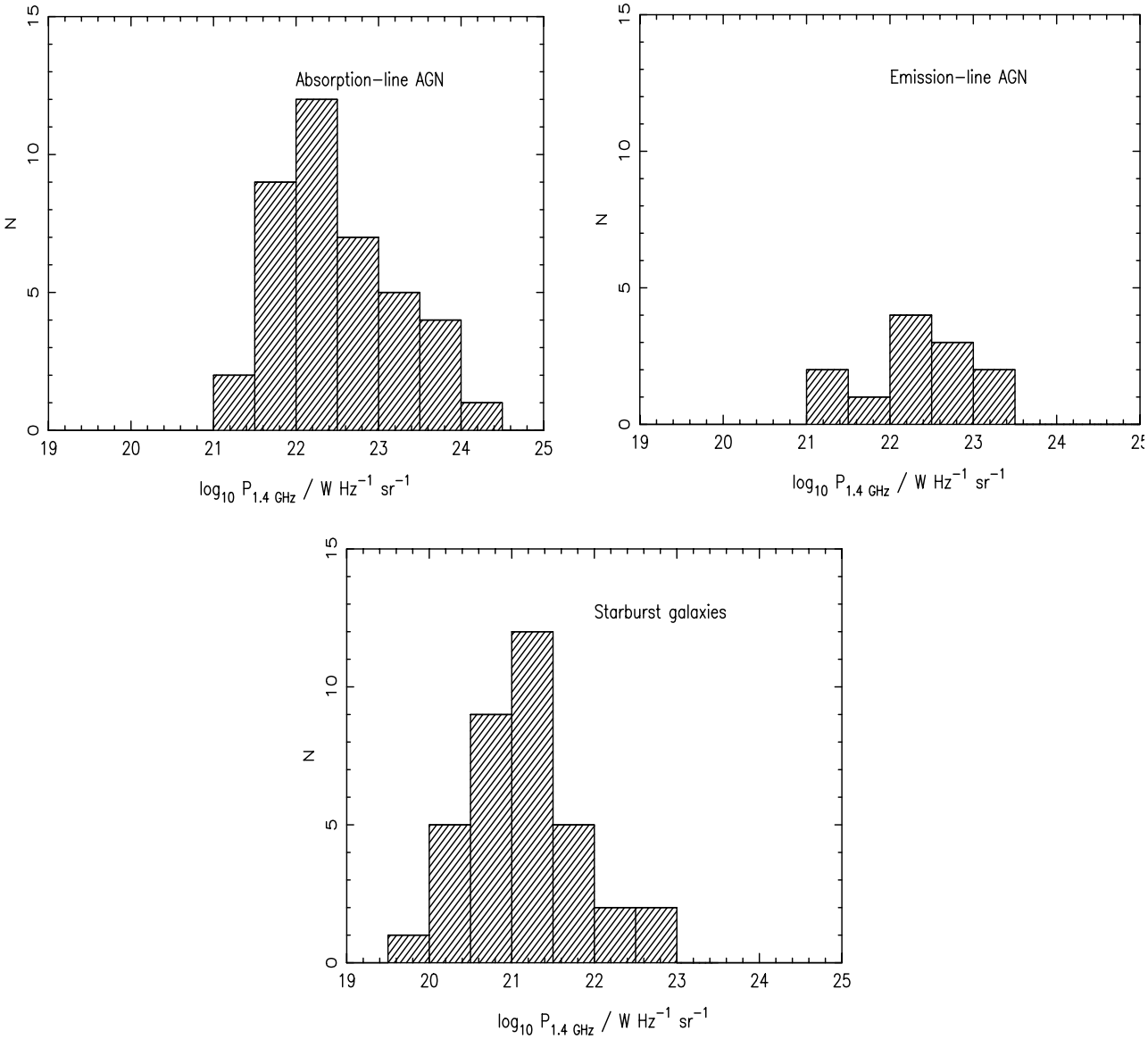

Figure 1—Luminosity distributions by type for the 88 2dFGRS–NVSS galaxies.

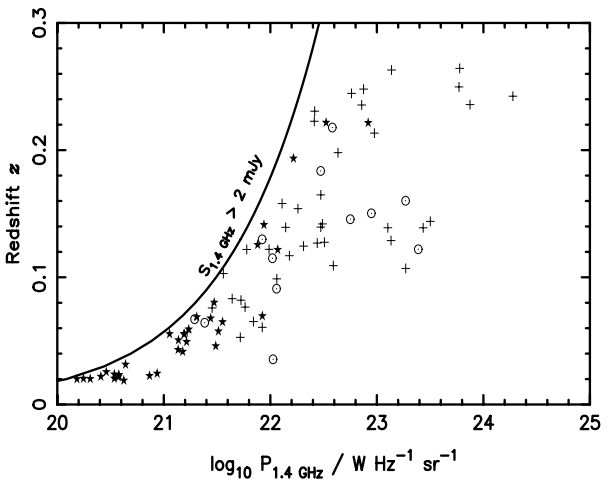

Figure 2—Radio power as a function of redshift for the sample of 88 2dFGRS–NVSS galaxies. Symbols show the initial galaxy classification types: ★ = starburst galaxy, ⊙ = emission-line AGN, + = absorption-line AGN.

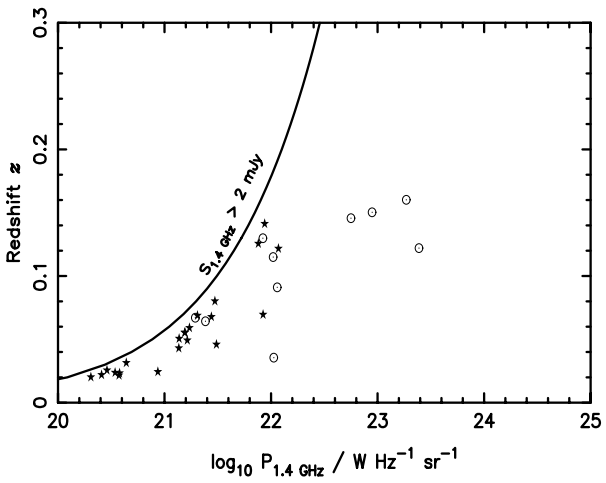

Figure 3—Radio power as a function of redshift for the 32 narrow-emission-line 2dFGRS–NVSS galaxies. Symbols show the initial galaxy classification types: ★ = starburst galaxy, + = emission-line AGN.

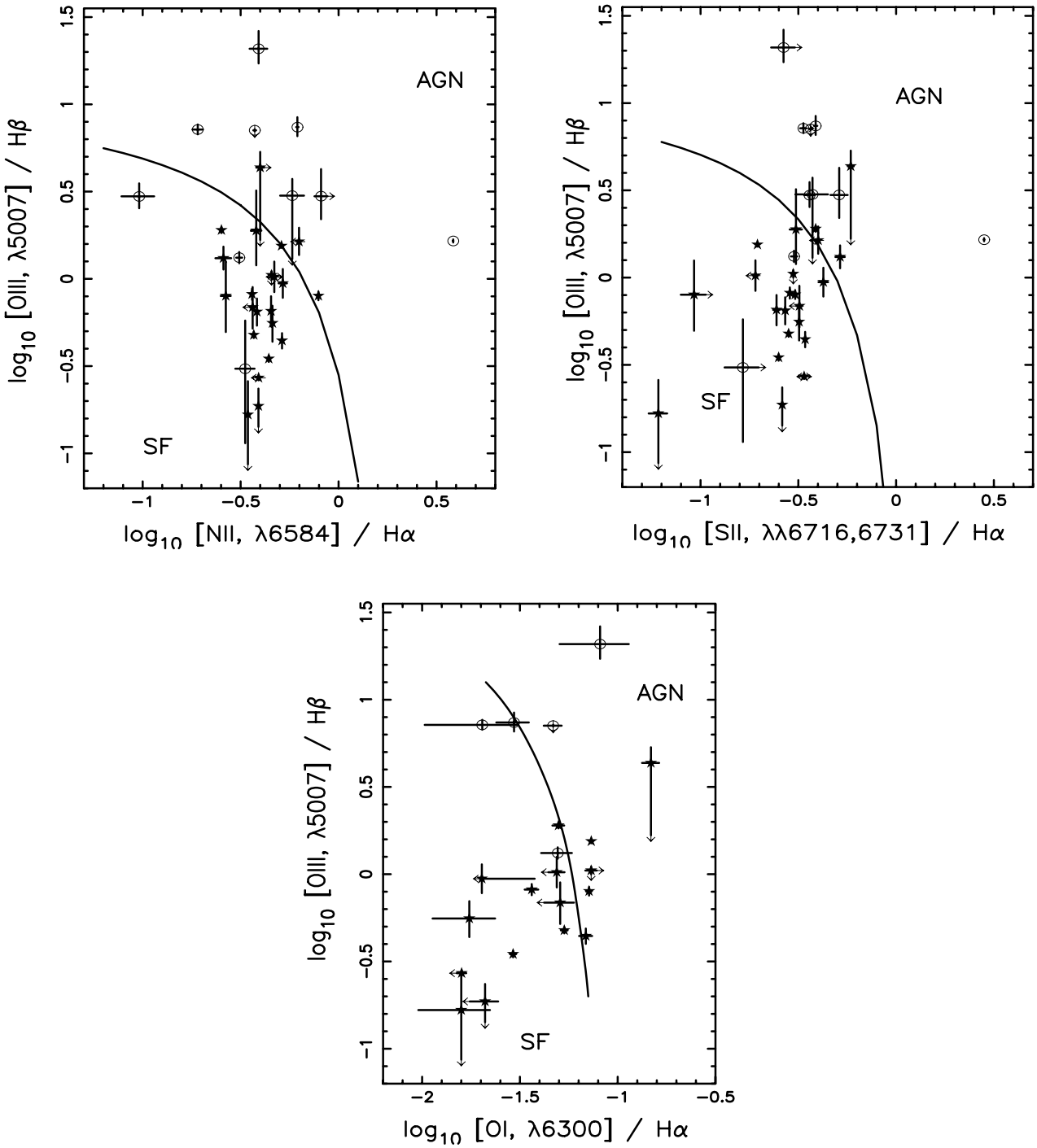

Figure 4—Diagnostic emission-line diagrams for the narrow-line galaxy sample. The symbols reflect the spectral types assigned by Sadler et al. (1999): ⊙ = AGN, ★ = starburst. The solid curves in the [NII] and [SII] plots are from Kewley et al. (2000), whilst the solid curve in the [OI] plot is from Veilleux & Osterbrock (1987). These curves divide non-thermal emission-line characteristics ('AGN') from thermal ('starburst galaxies', characterised by OB stars). Error bars have been calculated from the S/N ratio in each spectrum and the effects of residual night-sky features. Upper and lower limits are marked with arrows.

AGN with Balmer-line emission form our 'narrow-line galaxy sample'.

Figure 2 shows the distribution of radio power with redshift for the sample of galaxies. The starburst galaxies cluster at low redshifts due to the flux density limit of the NVSS. The AGN generally lie at higher redshifts and radio powers. The highest-power objects are absorption-line AGN.

3 Emission-line Diagnostic Analysis

We determine the emission-line ratios for the narrow-line galaxy sample using the lines of Hα, Hβ, [OIII], [NII], [SII] and [OI]. Figure 3 shows the distribution of radio powers and redshifts for this sample. Comparing this distribution to those in Figure 1, we find we have an unbiased (P–z) subset of the complete sample.

Table 1. Emission-line ratios

2dFGRS Galaxy ID	b_J	Redshift	$\log_{10}(P_{1.4\ \mathrm{GHz}})$†	Measured line ratios [OIII]/Hα	[NII]/Hα	[SII]/Hα	[OI]/Hα
Initial classification SF							
TGS166Z108	17.2	0.0801	21.5	0.477±0.020	0.369±0.003	0.282±0.003	0.053±0.002
TGS206Z164	14.6	0.0255	20.5	1.887±1.324	0.380±0.024	0.307±0.023	
TGS206Z015	17.4	0.0685	21.9	1.544±0.040	0.511±0.002	0.195±0.002	0.073±0.002
TGS232Z060	16.8	0.0590	21.2	0.443±0.046	0.514±0.007	0.342±0.007	0.069±0.005
TGS235Z125	14.8	0.0243	20.9	<0.167±0.093	0.345±0.008	0.061±0.007	0.016±0.006
TGS236Z095	17.6	0.1420	20.6	<0.187±0.048	0.390±0.005	0.262±0.004	<0.021±0.003
TGS236Z091	17.0	0.0552	21.2	0.687±0.210	<0.364±0.012	<0.320±0.011	<0.051±0.009
TGS236Z194	15.5	0.0237	20.5	0.557±0.144	0.459±0.009	0.319±0.008	0.017±0.006
TGS238Z047	16.5	0.0215	20.6	0.271±0.009	<0.391±0.001	0.338±0.001	0.016±0.001
TGS238Z180	17.2	0.1255	21.9	0.942±0.197	0.519±0.026	0.424±0.024	<0.020±0.017
TGS239Z196	14.8	0.0219	20.4	0.798±0.455	0.266±0.016	>0.093±0.014	
TGS318Z156	18.3	0.0687	21.3	0.799±0.047	0.789±0.004	0.305±0.003	0.071±0.002
TGN218Z230	15.9	0.0201	20.3	0.654±0.142	0.452±0.011	0.245±0.010	
TGN220Z065	17.3	0.0492	21.2	<4.340±1.000	>0.398±0.018	0.586±0.021	0.148±0.015
TGN222Z132	16.7	0.0505	21.1	1.633±0.329	<0.628±0.009	<0.400±0.008	
TGN231Z143	15.5	0.0314	20.6	0.647±0.124	0.383±0.007	0.271±0.007	
TGN239Z061	17.5	0.0554	21.2	1.902±0.076	0.252±0.004	0.387±0.005	0.050±0.003
TGN239Z082	18.8	0.1412	21.9	<1.050±0.054	0.455±0.007	0.298±0.006	>0.073±0.005
TGN239Z221	17.4	0.0430	21.1	0.349±0.015	0.440±0.002	0.251±0.001	0.029±0.001
TGN239Z172	16.2	0.0459	21.5	1.026±0.229	0.470±0.007	<0.191±0.005	<0.049±0.005
TGN240Z019	19.3	0.1216	22.1	1.314±0.216	0.258±0.024	0.517±0.029	
TGN309Z233	17.9	0.0677	21.4	0.817±0.062	0.361±0.004	0.286±0.004	0.036±0.003
Initial classification AGN							
TGS207Z011	14.2	0.0355	22.0	1.649±0.035	3.845±0.014	2.817±0.011	0.553±0.004
TGS218Z173	18.6	0.0911	22.1	7.170±0.499	0.191±0.012	>0.335±0.013	0.020±0.010
TGS220Z128	18.9	0.1298	21.9	20.817±5.495	0.391±0.042	>0.265±0.038	0.081±0.033
TGS233Z084	18.4	0.0643	21.4	2.972±0.554	0.096±0.019	0.361±0.023	
TGS234Z066	18.9	0.1503	22.9	<7.101±0.098	0.373±0.006	0.366±0.006	0.047±0.005
TGS313Z081	17.7	0.1220	23.4	0.306±0.271	0.334±0.039	>0.165±0.034	
TGS313Z100	17.1	0.1457	22.8	<3.000±0.741	0.580±0.086	0.374±0.075	
TGN231Z211	16.4	0.0671	21.3	7.402±1.041	0.616±0.009	0.388±0.008	0.029±0.006
TGN239Z017	18.4	0.1150	22.0	2.976±1.282	>0.814±0.064	0.511±0.054	
TGN238Z202	19.3	0.1602	23.3	1.323±0.103	0.311±0.011	0.301±0.011	0.049±0.009

†Units W Hz^{-1} sr^{-1}

Even though the 2dFGRS spectra are not flux-calibrated, the pairs of emission lines were originally chosen to be close in wavelength. The line ratios are therefore accurately determined even for our uncalibrated spectra. The flux in each emission line is measured using the NOAO IRAF splot routine, fitting a Gaussian function to each emission feature. Diagnostic line ratios for [NII]λ6583/Hα, [SII]λλ6716,6731/Hα and [OI] λ6300/Hα are plotted in Figure 4 and the data summarised in Table 1.

The diagnostic diagrams reveal that the majority of our narrow-line galaxy sample have [NII]λ6583/Hα, [SII] λ6716+λ6731/Hα and [OI] λ6300/Hα ratios that straddle the region dividing AGN and starburst galaxies.

Table 2. Emission-line ratio classifications

2dFGRS Galaxy ID	Mag b_J	Redshift	$\log_{10}(P_{1.4\,\mathrm{GHz}})$†	Line ratio classification [NII]/Hα	[SII]/Hα	[OI]/Hα
Initial classification SF						
TGS166Z108	17.2	0.0801	21.5	S	S	S
TGS206Z164	14.6	0.0255	20.5	S?	S?	...
TGS206Z015	17.4	0.0685	21.9	?	S	A
TGS232Z060	16.8	0.0590	21.2	S	S	?
TGS235Z125	14.8	0.0243	20.9	S	S	S
TGS236Z095	17.6	0.1420	20.6	S	S	S
TGS236Z091	17.0	0.0552	21.2	S	S	S
TGS236Z194	15.5	0.0237	20.5	S	S	S
TGS238Z047	16.5	0.0215	20.6	S	S	S
TGS238Z180	17.2	0.1255	21.9	S	S	S
TGS239Z196	14.8	0.0219	20.4	S	S	...
TGS318Z156	18.3	0.0687	21.3	?	S	A
TGN218Z230	15.9	0.0201	20.3	S	S	...
TGN220Z065	17.3	0.0492	21.2	A?	A	A
TGN222Z132	16.7	0.0505	21.1	A	?	...
TGN231Z143	15.5	0.0314	20.6	S	S	...
TGN239Z061	17.5	0.0554	21.2	S	?	?
TGN239Z082	18.8	0.1412	21.9	S	S	A
TGN239Z221	17.4	0.0430	21.1	S	S	S
TGN239Z172	16.2	0.0459	21.5	S	S	S
TGN240Z019	19.3	0.1216	22.1	S	A	...
TGN309Z233	17.9	0.0677	21.4	S	S	S
Initial classification AGN						
TGS207Z011	14.2	0.0355	22.0	A	A	A
TGS218Z173	18.6	0.0911	22.1	A	A	S
TGS220Z128	18.9	0.1298	21.9	A	A	A
TGS233Z084	18.4	0.0643	21.4	S	A	...
TGS234Z066	18.9	0.1503	22.9	A	A	A
TGS313Z081	17.7	0.1220	23.4	S	S	...
TGS313Z100	17.1	0.1457	22.8	A?	A?	...
TGN231Z211	16.4	0.0671	21.3	A	A	?
TGN239Z017	18.4	0.1150	22.0	A	A	...
TGN238Z202	19.3	0.1602	23.3	S	S	S

†Units W Hz^{-1} sr^{-1}

This is in contrast to optically-selected galaxy samples, whose narrow-line emission characteristics clearly delineate those with a hard ionising radiation source (AGN: right-hand side of curves in Figure 4) and those with hot OB stars (starburst, left-hand side of curves). Similar results to our line ratio distribution have been found for other radio-selected samples (e.g. Georgakakis et al. 1999) as well as IR-selected galaxy samples (Kewley et al. 2000).

In Table 2 we show how the galaxies are classified based on the individual emission-line ratio values. Where the errors associated with the line ratio span the empirical dividing line, the classification is given as A?

or S?. For the cases where the ratio lies right on the dividing line, the classification is given as ?.

We find four galaxies with different line ratio classifications to the 'eyeball' classifications of Sadler et al. (1999):

(1) TGN220Z065: Starburst galaxy, line ratio diagnostics indicate that it is an AGN. However, the Hβ measurement is a lower limit so that the the [OIII]/Hβ value is overestimated.

(2) TGN222Z132: Starburst galaxy, line ratio diagnostics indicate that it is an AGN. However, the Hα measurement is a lower limit so that the [SII]/Hα value is overestimated.

(3) TGN238Z202: AGN galaxy, line ratio diagnostics indicate that it is a starburst galaxy. Re-examining the 2dFGRS spectrum shows dominant Balmer lines characteristic of a starburst galaxy.

(4) TGS313Z081: AGN galaxy, line ratio diagnostics indicate that it is a starburst galaxy. Re-examining the 2dFGRS spectrum reveals strong Hα, weak Hβ and the 5577 Å line coincident with [OIII, 5007Å]. On balance this probably should be classified as a starburst galaxy.

Thus the diagnostic line ratios confirm 30 out of 32 of the 'eyeball' classifications. However, the frequency of ambiguous classifications from the line ratio diagnostics (indicated as A?, S? and ? in Table 3 below) indicates that a radio-selected sample does not clearly separate into the starburst and AGN regions defined by optically-selected samples.

Table 3. Star formation rates from IR and radio flux densities

2dFGRS Galaxy ID	$\log_{10}(P_{1.4\ \mathrm{GHz}})$†	Star formation rate $M \geq 5\ M_{\odot}\mathrm{yr}^{-1}$	
		$\mathrm{Radio}_{1.4\ \mathrm{GHz}}$	$\mathrm{IR}_{60\ \mu\mathrm{m}}$
TGS166Z108	21.5	9.3	7.1
TGS206Z164	20.5	0.9	0.7
TGS206Z015	21.9	26.4	77.7
TGS232Z060	21.2	5.4	4.2
TGS235Z125	20.9	2.7	2.1
TGS236Z095	20.6	1.2	1.1
TGS236Z091	21.2	4.9	2.9
TGS236Z194	20.5	1.1	1.0
TGS238Z047	20.6	1.2	1.3
TGS238Z180	21.9	23.9	11.0
TGS239Z196	20.4	0.8	0.5
TGS318Z156	21.3	6.4	8.8
TGN218Z230	20.3	0.6	0.6
TGN220Z065	21.2	5.1	2.6
TGN231Z143	20.6	1.4	1.0
TGN239Z061	21.2	4.3	4.3
TGN239Z172	21.5	9.7	7.4

†Units W Hz^{-1} sr^{-1}

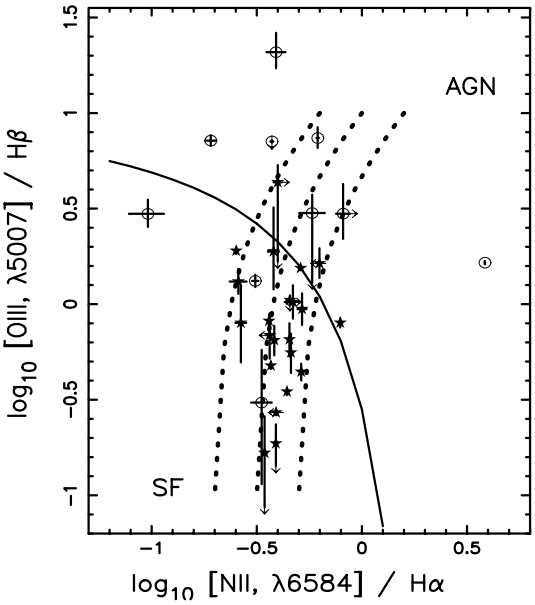

Figure 5—Diagnostic emission-line ratios for [NII]/Hα as shown in Figure 4. The solid line divides the starburst (SF) and AGN sources from Kewley et al. (2000). Mixing lines are shown as dotted lines, with increasing AGN contributions lying at higher [OIII]/Hβ values.

Further evidence as to the composite nature of the starburst galaxies can be found by comparing the star-formation rates indicated by the radio and IR flux densities. Table 3 shows the flux densities and the implied star formation rates for massive stars (>5$M_{\odot}$, Cram et al. 1998), using 60 μm flux density data compiled by Sadler et al. (1999) from the IRAS Point Source and Faint Source catalogues. Two galaxies stand out as having very discrepant implied star formation rates: (1) TGS206Z015 has an IR excess, and (2) TGS238Z180 has a radio excess. In both cases the UKST IIIaJ images show that the galaxies are undergoing mergers, which is possibly enhancing or triggering starburst activity in these objects.

Furthermore, we suggest that the majority of the narrow-line galaxies whose line ratios are strung out between the two regions (star-forming and AGN) are composite galaxies: the individual line ratios lie along mixing lines whose positions on the diagnostic plots are determined by the admixture of AGN and starburst components, as shown in Figure 5.

4 Summary

Our analysis finds that this preliminary sample of narrow-emission-line galaxies selected from 2dFGRS and NVSS comprises a mix of starburst and AGN types. The distribution of their emission-line ratios suggests that a sizable fraction of the galaxies may be composite galaxies. Further work will determine the relative contributions of the star-forming and AGN components.

Acknowledgments
We thank the 2dF Galaxy Redshift Survey team for advance access to their data. DML thanks the Science Foundation for Physics at the University of Sydney for a summer vacation scholarship.

References

Bock, D. C.-J., Large, M. I., & Sadler, E. M. 1999, AJ, 117, 1578
Colless, M. M. 1999, Phil. Trans. R. Soc. Lond., 357, 105
Condon, J. J., Cotton, W. D., Greisen, E. W., Yin, Q. F., Perley, R. A., & Broderick, J. J. 1998, AJ, 115, 1693
Cram, L., Hopkins, A., Mobasher, B., & Rowan-Robinson, M. 1998, ApJ, 507, 155
Georgakakis, A., Mobasher, B., Cram, L., Hopkins, A., Lidman, C., & Rowan-Robinson, M. 1999, MNRAS, 306, 708
Kewley, L., Heisler, C. A., Dopita, M. A., & Lumsden, S. 2001, ApJ5, 132, 37
Sadler, E. M., McIntyre, V. J., Jackson, C. A., & Cannon, R. D. 1999, PASA, 16, 247
Veilleux, S., & Osterbrock, D. E. 1987, ApJS, 63, 295
White, R. L., Becker, R. H., Helfand, D. J., & Gregg, M. D. 1997, ApJ, 475, 479